

Effect of nickel precursors on the performance of Ni/AlMCM-41 catalysts for *n*-dodecane hydroconversion

Kegong Fang, Jie Ren, Yuhan Sun*

State Key Laboratory of Coal Conversion, Institute of Coal Chemistry, Chinese Academy of Sciences, Taiyuan 030001, PR China

Received 20 November 2003; received in revised form 28 October 2004; accepted 28 October 2004

Available online 21 December 2004

Abstract

The bifunctional Ni/AlMCM-41 catalysts with 2.0 wt.% nickel loading were prepared by means of the wetness impregnation technique using three nickel precursors: nickel nitrate, alkaline tetraamine nickel nitrate and nickel citrate. The texture, crystal phase and surface metal/acidity functions were characterized by the techniques such as N₂-sorption, XRD, XPS, H₂-chemisorption, FT-IR and NH₃-TPD. It was shown that the catalyst prepared with nickel citrate exhibited stronger metal–support interaction and higher metal dispersion than those prepared with nickel nitrate and alkaline tetraamine nickel nitrate. The intimate metal–acid interaction and the enhanced (de)hydrogenating capability of this catalyst led to the highest catalytic activity and isomerization selectivity in *n*-dodecane hydroconversion.

© 2004 Elsevier B.V. All rights reserved.

Keywords: AlMCM-41; Nickel precursor; Bifunctional catalyst; *n*-Dodecane hydroconversion

1. Introduction

Nickel-supported catalysts are widely used in various important industrial hydrogenation processes such as hydrocracking and hydroisomerization of *n*-paraffin [1–3]. Over these catalysts, the hydrocarbons are dehydrogenated (hydrogenated) on the metallic nickel active sites, while isomerization and cracking occurred on the Brønsted acid sites of the support [4,5]. This determined that the proper acid/metal balance is critical for obtaining ideal hydroisomerization-cracking behavior of hydrocarbons.

The typical supports used in the *n*-paraffin hydroconversion are amorphous acidic oxides, zeolites, etc. [6–8]. Based on these materials, the nickel catalysts have gained important applications in petrochemical industry for the purpose of producing high-quality gasoline and improving the low-temperature properties such as the pour point of diesel fuels as well as lube oils [2,7]. However, these catalysts have more or less shortcomings such as sensitivity to deactivation

by coking, large production of gases by excess cracking or pore opening restrictions for large molecules [9]. Thus, there is more desired to seeking novel bifunctional catalysts with improved stability and diffusion transfer capacity in the conversion of heavy paraffin fractions.

The discovered mesoporous MCM-41 aluminosilicate, possessing high surface area, tunable uniform mesopores and mild acidity, might be a good candidate to design the bifunctional catalyst used in the conversion of long chain paraffins [10,11]. Till now, various bifunctional nickel catalysts supported on mesoporous AlMCM-41 materials have been prepared and extensively characterized [12–27]. The most widely used method is impregnation or ion-exchange with different nickel salt solutions, such as nickel nitrate [12–17,21,23–26], nickel chloride [16,17] or amine nickel nitrates [22]. Usually, the catalysts prepared in such above methods contained some larger nickel particles on the external surface of the supports. To improve the nickel dispersion over the MCM-41 support, direct adding the nickel salt into the synthesis solution of MCM-41 has been tried to incorporate the nickel atoms into the framework wall of the support, but the mesostructure is heavily distorted even at

* Corresponding author. Tel.: +86 351 4041627; fax: +86 351 4050320.
E-mail address: yhsun@sxicc.ac.cn (Y. Sun).

very low nickel contents of 1.5 wt.% [17,22]. Recently, alternative preparation method of Ni-containing MCM-41 catalysts using a non-crystalline, film-forming nickel citrate has been developed [28–31]. Lensveld et al. have impregnated nickel citrate aqueous solution onto the pure-silica MCM-41 and gained highly dispersed nickel oxide particles [28]. Also, Eliche-Quesada et al. reported that the use of nickel citrate as the nickel source could effectively inhibit the aggregation of nickel particles on the surface of the zirconium-doped MCM-41 [31]. These studies largely extended the preparation of nickel-containing MCM-41 catalysts and some of the catalysts are successfully applied in the oligomerization of olefin [32], (de)hydrosulfurization and hydrogenations [14,23,26,33]. However, the catalytic applications of these catalysts in the hydroconversion of long-chain paraffins are still limited [12,34–36].

In the present study, we have prepared several Ni/AlMCM-41 catalysts using the wetness impregnation method and investigated the effect of nickel salt precursors on the catalytic performance in *n*-dodecane hydroconversion. The crystalline phase, textural properties and surface metal–acid functions were characterized using various techniques. Based on the characterization results, the correlations between the catalytic performance and the surface metal–acid functions were further studied.

2. Experimental

2.1. Catalyst preparation

Mesoporous aluminosilicate (AlMCM-41 with Gel Si/Al = 15) was hydrothermally synthesized by modifying the procedure reported in open literature [37]. Sodium aluminate (41% Al₂O₃) was dissolved in demineralised water and mixed with a certain amount of silicate anions solution (28.8% SiO₂, 10.8% Na₂O). Then the cetyltrimethylammoniumbromide (CTAB) aqueous solution was added to the above mixture with stirring. Subsequently, the pH of the gel mixture was adjusted to ca. 10.3 by dropwise addition of 2 M HCl. The resulting gel with molar composition 1.0SiO₂:0.41Na₂O:0.033Al₂O₃:0.2CTAB:80H₂O was transferred to a teflon-lined autoclave and aged at 393 K for 48 h. The solid product recovered by filtration was washed with deionized water, dried in air at 333 K and calcined at 873 K for 5 h to get the template-free AlMCM-41. The protonated form of AlMCM-41 was obtained by ion exchange with 1 M NH₄NO₃ solutions twice at 323 K for 8 h, dried at ambient temperature, and then calcined at 813 K for 3 h.

The nickel-supported catalysts were prepared by the wetness impregnation technique using three different nickel precursors: nickel nitrate, alkaline tetraamine nickel nitrate and nickel citrate. Nickel citrate was prepared by mixing nickel carbonate and citric acid with a 3:2 molar ratio in deionized water as described by Lensveld et al. [28]. In all cases, a certain amount of nickel precursor solutions was impregnated

onto the AlMCM-41 support to get the 2.0 wt.% Ni loading. After impregnation, the catalysts were dried at 393 K for 5 h and calcined at 673 K for 4 h in air.

2.2. Characterization

X-ray powder (XRD) measurement was carried out using a Philips PW 1050/25 diffractometer with Cu K α radiation (50 kV, 30 mA). The textural properties of the samples were determined in a Micromeritics TriStar 3000 automated nitrogen physisorption apparatus.

Ammonia temperature-programmed desorption (NH₃-TPD) was measured by a flow system with a thermal conductivity detector. The reduced catalyst (150 mg) was outgassed in argon flow, heated to 873 K with 10 K/min, and kept for 30 min. The sample was cooled down to 373 K and adsorbed by flowing NH₃/Ar stream for 10 min. After equilibration in argon flow for 1 h at 373 K, the catalyst was again heated at a linear rate of 10 K/min to 873 K, and then the desorbed ammonia were monitored by an online gas chromatograph equipped with a thermal conductivity detector.

FT-IR spectra of pyridine adsorption were recorded on a Nicolet Magna 550 Fourier transform infrared spectrometer at 4 cm⁻¹ resolution. The sample was finely grounded and pressed into self-supporting wafer (10 mg/cm², diameter = 15 mm), and then placed into the measurement cell with CaF₂ windows. The sample was first reduced by hydrogen, and then evacuated at 773 K (ca. 10⁻⁴ Torr) for 4 h prior to adsorption of pyridine. IR spectra were recorded after subsequent evacuation at 433 K.

The temperature-programmed reduction (TPR) of the samples was performed in a flow system with a thermal conductivity detector. The samples (100 mg) were first outgassed in argon by heating to 773 K and then cooled at ambient temperature. Next, they were heated in an H₂/Ar (5/95 volumetric ratio) reducing gas mixture from room temperature to 1023 K by a heating rate of 10 K/min and the detector signal was recorded continuously.

X-ray photoelectron spectra (XPS) were recorded on a VG ESCALAB210 spectrometer equipped with an Mg K α radiation and a hemispherical electron analyzer. The powdered samples were pressed into an indium foil, reduced *ex situ* in H₂ at 773 K for 4 h, and then moved into the pretreatment chamber of the spectrometer under N₂ flow protection. Energy regions of the photoelectrons were scanned at pass energy of 25 eV. Peak intensities were estimated by calculating the integral of each peak, after smoothing, subtraction of the S-shaped background and fitting the curve to a combination of Lorentzian and Gaussian lines. Energy correction was performed using the C 1s line at 284.9 eV as a charge reference.

Nickel dispersion was measured by H₂ chemisorption in a Pulse Chemisorb 2700 micromeritics apparatus. The samples were preheated at 773 K for 4 h in H₂ flow, followed by cleaning with Ar flow at 773 K for 30 min. Then the chemisorption experiments were performed at room temperature.

2.3. Catalytic test

n-Dodecane hydroconversion was carried out in a down flow fixed-bed stainless steel tube reactor (i.d. = 6 mm; 120 cm in length) at 2.0 MPa and H₂/*n*-dodecane molar ratio of 20. The catalyst was pretreated in Ar flow and then reduced in situ in a flow of H₂ at 773 K for 4 h prior to the start of the reaction. The gas products were analyzed by gas chromatograph with a GDX-103 column and FID detector, an OV-101 capillary column and FID detector for the liquid ones.

3. Results and discussion

3.1. Textural and phase structure

Fig. 1 showed the XRD patterns of the samples. The AlMCM-41 support exhibited only a broad (100) peak at $2\theta = 2.2^\circ$, while other diffraction peaks corresponding to the (110) and (200) crystal plans were unresolved due to the large amount of aluminum incorporation [38,39]. After nickel impregnation, the intensity of the (100) peak decreased, indicating that the distortion of the mesostructure took place. The N₂ sorption isotherms and the textural properties of the samples were given in Fig. 2 and Table 1, respectively. The AlMCM-41 support showed a type IV isotherm, typical of mesoporous MCM-41 materials [40]. Upon nickel impregnation with nickel nitrate and nickel citrate aqueous solutions, the shape of the isotherm hardly changed and the textural properties (surface area, pore volume and average pore size) reduced slightly. However, when the AlMCM-41 support was soaked with alkaline tetraamine nickel nitrate solution, the capillary condensation step became less steep and the surface area markedly decreased, indicating that the structure of AlMCM-41 was more readily destroyed in the alkaline nickel salt aqueous solution. This result could be explained by the interaction between the hydroxide and the AlMCM-41 support. In the tetraamine nickel nitrate solution, the silanol groups on the surface of AlMCM-41 were attacked by a large

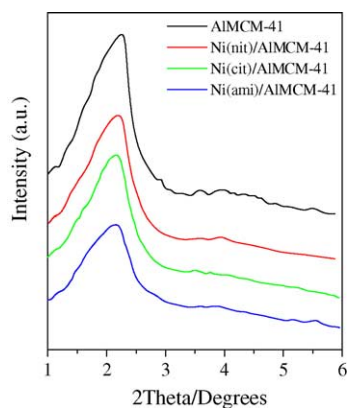


Fig. 1. Powder XRD patterns of the samples.

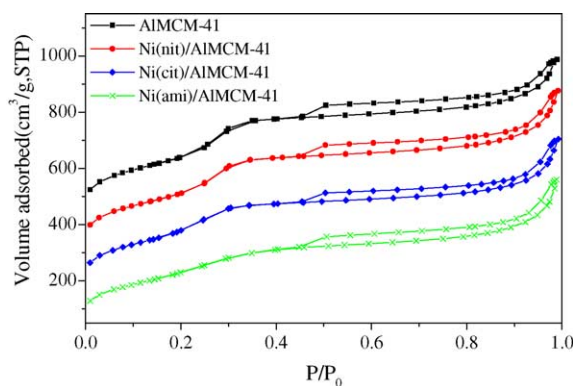


Fig. 2. N₂ adsorption/desorption isotherms of the samples.

amount of hydroxides via S_N2 mechanism [41], causing the cleavage of the Si–O bonds and further collapse of the framework of AlMCM-41 during the hydrolysis course. Contrary to this, the existence of hydrogen cations in the nickel nitrate and nickel citrate aqueous solutions could protect the mesostructure from being attacked by the hydroxides in some extent. Therefore, the mesostructure of AlMCM-41 was mainly retained after impregnation by nickel nitrate and nickel citrate aqueous solutions.

3.2. Reducibility and metal dispersion

The H₂-TPR profiles of the catalysts (Fig. 3) showed a broad peak at 820–890 K, shouldered with a small peak at 660–690 K, indicating that there were two different nickel species presented on the surface of the catalysts. The small shoulder peak at low temperature coincided with the reduction of the large bulk NiO particles [28], which were probably located at the external surface of the support. The second H₂ consumption peak at higher temperature originated from the reduction of the small nickel oxide species, chemically bounded with the AlMCM-41 framework [26]. All the catalysts mainly contained small nickel oxide particles, which were revealed by the rather large area of the second H₂ consumption peak. The reduction peak of Ni(cit)/AlMCM-41 catalyst maximum at the highest temperature among the three

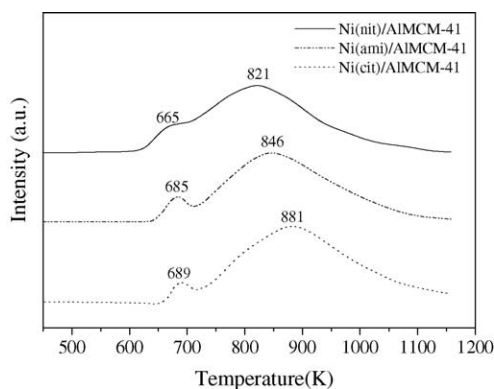


Fig. 3. H₂-TPR profiles of the catalysts.

Table 1
Textural properties of the Ni/AlMCM-41 catalysts

Catalysts	Precursor	S_{BET} (m^2/g)	Pore volume (cm^3/g)	APD ^a (\AA)
AlMCM-41		895	0.80	36.7
Ni(nit)/AlMCM-41	$\text{Ni}(\text{NO}_3)_2$	867	0.77	36.5
Ni(ami)/AlMCM-41	$[\text{Ni}(\text{NH}_3)_4](\text{NO}_3)_2$	775	0.69	34.7
Ni(cit)/AlMCM-41	$\text{Ni}_3(\text{Cit})_2$	855	0.73	35.6

^a Average pore diameter.

catalysts, indicating that the nickel-support interaction was strongest and the nickel oxide particles were highly dispersed in the case of Ni(cit)/AlMCM-41 catalyst.

XPS analysis was used to study the nature of the surface species. All the prereduced catalysts showed the similar XPS spectra (see Fig. 4). The Ni 2p core level signal of the catalysts showed a broad Ni 2p_{3/2} profile at about 852–857 eV, which could be deconvoluted into three components. The peak at ca. 852.3 eV corresponded to the Ni⁰ species, two other peaks at 855.3 and 857.2 eV could be associated with the octahedral Ni²⁺ and the very small crystallites of NiO located on the framework wall of the mesostructure [31]. The peak area of Ni⁰ signal was much smaller than that of NiO signals, indicating that only a small fraction of NiO was reduced. This might lead us to consider that the NiO species on the surface of the AlMCM-41 was in the form of charged clusters, strongly interacted with the support, and then the charged NiO species were rather difficult to be reduced. The signal with the binding energy at 861.7 eV corresponded to the shake-up satellite structure of Ni²⁺ [31,42]. The NiO emission lines of the Ni(cit)/AlMCM-41 catalyst slightly shifted to the higher binding energy values than those of Ni(nit)/AlMCM-41 and Ni(ami)/AlMCM-41 catalysts, indicating the stronger metal–support interaction of the former catalyst. The quantitative XPS analysis results were compiled in Table 2. The reduction degree ($\text{Ni}^0/\text{Ni}_{\text{total}}$) of the catalysts decreased in the order of Ni(nit)/AlMCM-41 > Ni(ami)/AlMCM-41 > Ni(cit)/AlMCM-41, which coincided with the expected results of H₂-TPR characterization.

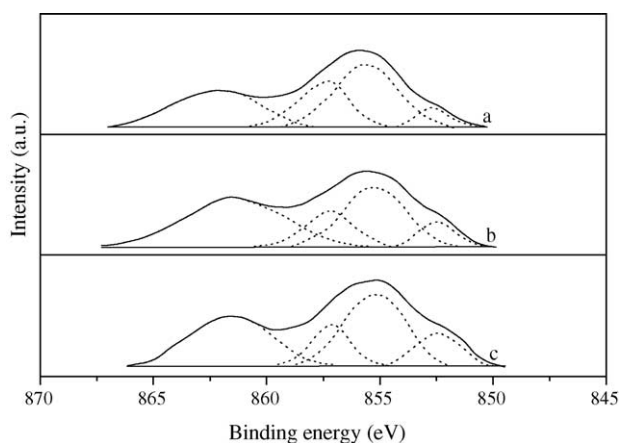


Fig. 4. Ni 2p XPS spectra of the reduced catalysts.

Table 3 showed the nickel dispersion of the catalysts obtained by H₂ chemisorption. The Ni(cit)/AlMCM-41 catalyst demonstrated the highest percentage of metal exposed on the total surface (external and inner surface) of AlMCM-41, whereas the Ni(ami)/AlMCM-41 and Ni(nit)/AlMCM-41 led to relatively lower nickel dispersion. This should be ascribed to the nature of nickel precursors. It was known that the nickel citrate precursor could leave a wetting, highly viscous film on the surface of the support upon solvent removal, which avoided the entrainment of Ni²⁺ ions from the mesopores of the support. After calcination, this thin film was broken up and decomposed, resulting in the formation of small nickel oxide particles with high dispersion [28]. By contrast, using the nickel nitrate or alkaline tetraamine nickel nitrate as nickel source, some Ni²⁺ ions could readily entrain out of the mesopores with the lower viscous solvents flow upon drying, and then aggregated each other, forming relatively larger nickel particles upon calcination. As a sequence, the nickel species could be well dispersed on the mesoporous AlMCM-41 support by using wetness impregnation with nickel citrate aqueous solution.

3.3. Acidity

The AlMCM-41 exhibited two desorption peaks in NH₃-TPD profile (see Fig. 5), corresponding to the weak and medium acid sites. After nickel incorporation onto the support, the prepared catalysts had the similar acid feature to that of AlMCM-41. However, the total acid sites of the catalysts increased in comparison with that of the support (see

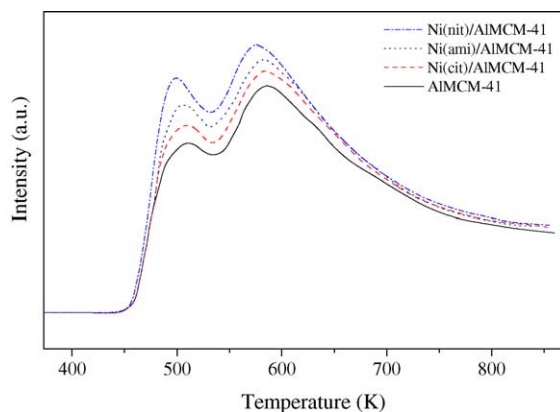


Fig. 5. NH₃-TPD curves of the samples.

Table 2
XPS analysis of the reduced Ni/AlMCM-41 catalysts

Catalysts	Binding energy (eV)			Surface atomic ratio	
	Al 2p	Ni 2p _{3/2}		Si/Al	Ni ⁰ /Ni _{total} (%)
		Ni ²⁺	Ni ⁰		
Ni(nit)/AlMCM-41	75.2	855.3, 857.2	852.3	10.8	18.2
Ni(ami)/AlMCM-41	75.3	855.4, 857.3	852.3	11.1	15.6
Ni(cit)/AlMCM-41	75.5	855.7, 857.3	852.5	11.2	11.7

Table 3
Acidity and metal properties of Ni/AlMCM-41 catalysts

Catalysts	Acidity ^a (mmol Py/g)			NH ₃ desorbed ^b (mmol/g)	D _{Ni} ^c (%)	n _{Ni} /n _A ^d
	B	L	B + L			
AlMCM-41	0.54	0.78	1.32	0.55	–	–
Ni(nit)/AlMCM-41	0.52	0.88	1.40	0.63	11.1	0.07
Ni(ami)/AlMCM-41	0.51	0.85	1.36	0.59	13.5	0.09
Ni(cit)/AlMCM-41	0.49	0.84	1.33	0.57	17.0	0.11

^a Calculated using the extinction coefficients by Emeis [47].

^b NH₃ desorbed beyond 373 K.

^c Nickel dispersion.

^d n_{Ni}/n_A is the ratio of exposed nickel atoms number to the Brønsted acid number.

Table 3). Combined with the Py-IR results (see Fig. 6), it could be seen that the Brønsted acid sites of the AlMCM-41 decreased while the Lewis acid sites were largely enhanced upon nickel impregnation (see Table 3), which ultimately caused the increase of the total acid sites. The nickel modification over the acidity of the support had two different effects [43–46]. The Ni species could cover some acid sites (both Brønsted and Lewis acid sites), causing the decrease of the total acid sites. On the other hand, the coordinately unsaturated nickel cations could serve as a kind of new Lewis acid centers, which compensated the original Lewis acid sites being covered. In the present case, the compensating effect of the Ni species override the covering one, which caused the increase of the total acid sites. Besides, the total acid sites of the catalysts increased in the order of Ni(cit)/AlMCM-41 < Ni(ami)/AlMCM-41 < Ni(nit)/AlMCM-41, which was

contrary to the sequence of the nickel dispersion on the surface of the catalysts. This might indicate that the covering effect of the nickel species was more apparent compared with the compensating effect at higher nickel dispersion.

3.4. Catalytic performance

The activities of the catalysts in the *n*-dodecane hydro-conversion versus temperature were shown in Fig. 7. In the temperature range of 573–633 K, the activities of the catalysts increased sharply as the temperature increased. However, the increase of the activities became moderate beyond 633 K. This was probably due to the near attainment of equilibrium for the isomerization reaction at higher temperature. At given reaction temperature, the activities of the catalysts increased in the following order: Ni(nit)/AlMCM-

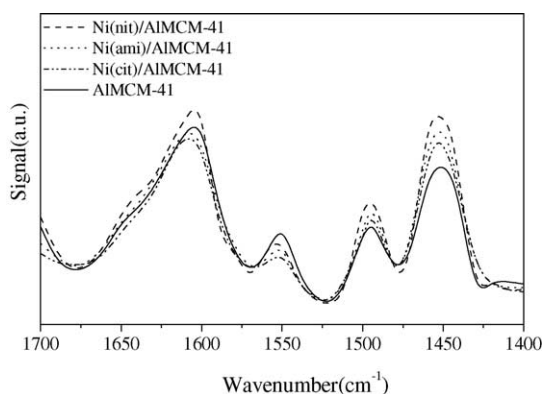


Fig. 6. IR spectra of pyridine adsorbed on the samples after being degassed at 433 K.

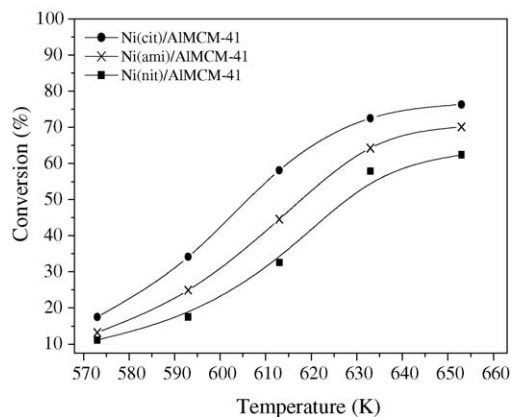


Fig. 7. *n*-Dodecane conversion as a function of temperature over Ni/AlMCM-41 catalysts.

Table 4
Composition of some cracked products on Ni/AlMCM-41 catalysts

Catalysts	$X_{n-C_{12}}$ (%)	C_3/C_1 (molar)	C_4-C_9 (mol%)	i/n (C_4-C_9) (molar)
Ni(nit)/AlMCM-41	40.3	19.8	86.4	2.2
Ni(ami)/AlMCM-41	44.4	18.8	85.9	2.1
Ni(cit)/AlMCM-41	47.9	15.6	85.7	1.9

$41 < \text{Ni(ami)/AlMCM-41} < \text{Ni(cit)/AlMCM-41}$, which was consistent with the sequence of nickel dispersion on the surface of the catalysts. This indicated that the activities of the catalysts mainly depended on the nickel dispersion. The higher dispersion of nickel particles might cause a closer interaction between acid and metal sites, and then more intermediates could be generated and further transferred between the two active sites. As a result, the Ni(cit)/AlMCM-41 catalyst with higher nickel dispersion showed better activity than the other catalysts.

The selectivity toward *i*-dodecane over the three catalysts decreased with the increase of conversion (see Fig. 8), which was commonly observed in the hydroisomerization-cracking of *n*-paraffins. However, the isomerization selectivity was always higher for the Ni(cit)/AlMCM-41 as compared with the other catalysts in the whole conversion range. According to the proposed bifunctional reaction mechanism for hydroisomerization and hydrocracking [48–50], the balance between metal and acid functions had great influence on the isomerization selectivity. Generally, the balance between metal and acid functions of the bifunctional catalysts was characterized by the ratio of the number of hydrogenating sites to the number of Brønsted acid sites ($n_{\text{Ni}}/n_{\text{A}}$). The higher the $n_{\text{Ni}}/n_{\text{A}}$ value was, the stronger (de)hydrogenating activity could be obtained over the catalyst. Therefore, the paraffins could be readily (de)hydrogenated over the Ni(cit)/AlMCM-41 catalyst due to its highest $n_{\text{Ni}}/n_{\text{A}}$ value in the three catalysts (see Table 3), which in turn suppressed the further cracking of the carbenium ions on the acid sites and then resulting in the highest isomerization selectivity.

The ratio of monobranched to multibranched dodecane isomers (M/B) as a function of the total conversion was

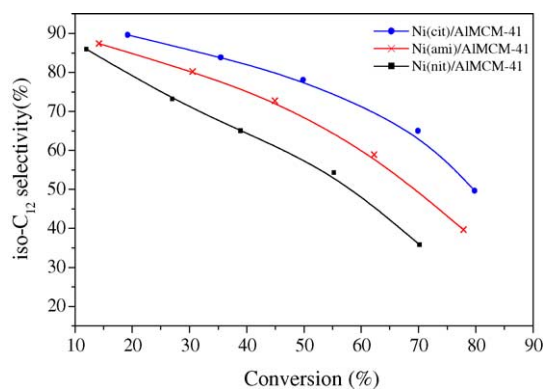


Fig. 8. Isomerization selectivity as a function of the conversion of *n*-dodecane.

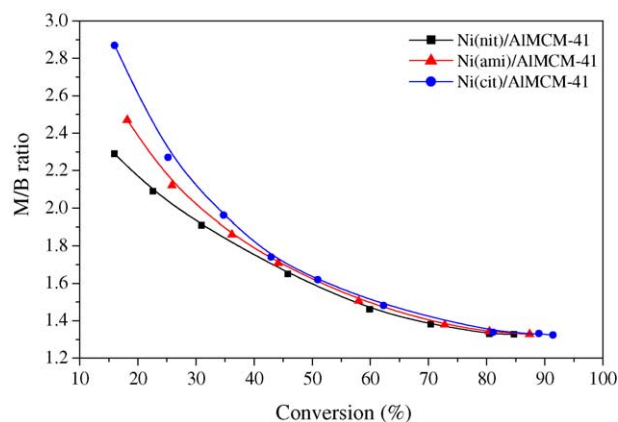


Fig. 9. The ratio of monobranched to multibranched dodecane isomers (M/B) as a function of conversion of *n*-dodecane.

shown in Fig. 9. In all cases, the M/B ratio declined with the increase of conversion, which was in line with the branching mechanism via protonated cyclopropanes [5,48,51]. At the same conversion, the M/B ratio decreased in the sequence of Ni(cit)/AlMCM-41 > Ni(ami)/AlMCM-41 > Ni(nit)/AlMCM-41, consistently with the $n_{\text{Ni}}/n_{\text{A}}$ value of the catalysts. Since the isomerization proceeded through successive branching from normal to mono- to multibranched dodecane [52], the higher $n_{\text{Ni}}/n_{\text{A}}$ value suggested that there was shorter residence time of the intermediate carbenium ions on the acid sites. Thus, the more monobranched carbenium ions could be transferred to the metal sites without further being branched.

Fig. 10 gave the carbon number distribution of the hydrocracking products at conversion of ca. 45%. The major

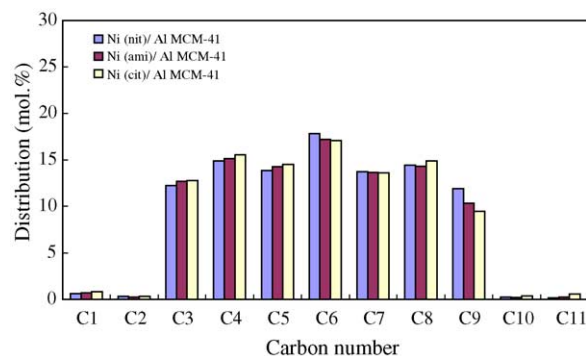


Fig. 10. Distribution of the cracked products over Ni/AlMCM-41 catalysts at the conversion of ca. 45%.

cracked products were C₃–C₉ hydrocarbons and the similar carbon number distribution was symmetrical centered at C₆ over the three catalysts, indicating that *n*-dodecane carried out a nearly ideal hydrocracking behavior. Besides, a trace of hydrogenolysis reaction might occur on the nickel metal surface because there were a very small amount of C₁+C₂ and C₁₀+C₁₁ presented in the cracked products. The lower C₃/C₁ ratio and the more linear light hydrocarbons were obtained on the Ni(cit)/AIMCM-41 catalyst (see Table 4), which coincided with the enhanced metal/acid ratio and the degree of branching of the dodecane isomers prior to cracking as discussed above.

4. Conclusions

The bifunctional Ni/AIMCM-41 catalysts have been prepared by means of the wetness impregnation method using three different nickel precursors: nickel nitrate, alkaline tetraamine nickel nitrate and nickel citrate. The mesostructure of AIMCM-41 was more readily destroyed in the alkaline tetraamine nickel nitrate solution due to the existence of a large amount of hydroxides, which accelerated the hydrolysis reaction of the silanol groups. The catalyst prepared with nickel citrate as the precursor possessed stronger metal–support interaction, higher metal dispersion and slightly lower acidity than those prepared with nickel nitrate and alkaline tetraamine nickel nitrate. In the test of *n*-dodecane hydroconversion, this catalyst exhibited better activity and isomerization selectivity due to the intimate interaction between metal and acid functions and the improved (de)hydrogenating capability of the metallic nickel active sites.

Acknowledgement

The authors gratefully acknowledge the funding of this project by National Key Fundamental Research and Development Projects of China (Project ID G1999022402).

References

- [1] G. Kinger, A. Lugstein, R. Swagera, M. Ebel, A. Jentys, H. Vinek, *Micropor. Mesopor. Mater.* 39 (2000) 307.
- [2] M.D. Romero, J.A. Calles, A. Rodriguez, J.C. Cabanelas, *Ind. Eng. Chem. Res.* 37 (1998) 3846.
- [3] D. Li, F. Li, J. Ren, Y. Sun, 241 (2003) 15.
- [4] S.T. Sie, *Ind. Eng. Chem. Res.* 32 (1993) 403.
- [5] J.A. Martens, P.A. Jacobs, in: J.B. Moffat (Ed.), *Theoretical Aspects of Heterogeneous Catalysis*, Van Nostrand Reinhold, New York, 1990, p. 52.
- [6] G. Kinger, A. Lugstein, *Appl. Catal. A* 218 (2001) 139.
- [7] A. Coma, A. Martinez, S. Pergher, S. Peratello, C. Perego, G. Bellusi, *Appl. Catal. A* 152 (1997) 107.
- [8] V. Calemma, S. Peratello, C. Perego, *Appl. Catal. A* 190 (2000) 207.
- [9] K. Sato, Y. Iwata, T. Yoneda, A. Nishijima, Y. Miki, H. Shimada, *Catal. Today* 45 (1998) 367.
- [10] C.T. Kersge, M.E. Lenowicz, W.J. Roth, J.C. Vartuli, J.S. Beck, *Nature* 359 (1992) 710.
- [11] R. Mokaya, W. Jones, Z. Luan, M.D. Alba, J. Klinowski, *Catal. Lett.* 37 (1996) 113.
- [12] A. Coma, A. Martínez, V. Martínez-Soria, J.B. Montón, *J. Catal.* 153 (1995) 25.
- [13] T. Halachev, R. Nava, L. Dimitrov, *Appl. Catal. A* 169 (1998) 111.
- [14] J. Cui, Y.H. Yue, Y. Sun, W.Y. Dong, Z. Gao, *Stud. Surf. Sci. Catal.* 105 (1997) 687.
- [15] Y. Yue, Y. Sun, Z. Gao, *Catal. Lett.* 47 (1997) 167.
- [16] M. Hartmann, A. Pöppel, L. Kevan, *J. Phys. Chem.* 99 (1995) 17494.
- [17] M. Hartmann, A. Pöppel, L. Kevan, *J. Phys. Chem.* 100 (1996) 9906.
- [18] J.S. Jung, W.S. Chae, R.A. McIntyre, C.T. Seip, J.B. Wiley, C.J. O'Connor, *Mater. Res. Bull.* 34 (1999) 1353.
- [19] Y. Yue, Y. Sun, Q. Zu, Z. Gao, *Appl. Catal. A* 175 (1998) 131.
- [20] M. Ziolk, I. Novak, P. Keczyk, J. Kujawa, *Stud. Surf. Sci. Catal.* 177 (1998) 509.
- [21] T. Klimova, J. Ramírez, M. Calderón, J.M. Domínguez, *Stud. Surf. Sci. Catal.* 177 (1998) 509.
- [22] U. Junges, S. Disser, G. Schmid, F. Schüth, *Stud. Surf. Sci. Catal.* 117 (1998) 493.
- [23] M. Ziolk, I. Nowak, I. Sobczak, H. Poltorak, *Stud. Surf. Sci. Catal.* 130 (2000) 3047.
- [24] Y. Cesteros, P. Salagre, F. Medina, J.E. Sueiras, G.L. Haller, *Stud. Surf. Sci. Catal.* 135 (2001) 233.
- [25] M. Mandredi, A. Vaccari, E. Veggetti, M. Jacquín, D.J. Jonez, J. Rozière, *Appl. Catal. A: Gen.* 231 (2002) 263.
- [26] A. Lewandowska, S. Monteverdi, M. Bettahar, M. Ziolk, *J. Mol. Catal. A: Chem.* 188 (2002) 85.
- [27] J.S. Beck, C.T.-W. Chu, I.D. Johnson, C.T. Kresge, M.E. Leonowicz, W.J. Roth, J.C. Vartuli, *Appl. WO 91/11390*, 1991, Mobil Oil Corporation.
- [28] D.J. Lensveld, J. Gerbrand Mesu, A.J. van Dillen, K.P. de Jong, *Micropor. Mesopor. Mater.* 44–45 (2001) 401.
- [29] D.J. Lensveld, J. Gerbrand Mesu, A.J. van Dillen, K.P. de Jong, *Stud. Surf. Sci. Catal.* 143 (2002) 647.
- [30] A.J. van Dillen, R.J.A.M. Terörde, D.J. Lensveld, J.W. Geus, K.P. de Jong, *J. Catal.* 216 (2003) 257.
- [31] D. Eliche-Quesada, J. Mérida-Robles, P. Maireles-Torres, E. Rodríguez-Castellón, A. Jiménez-López, *Langmuir* 19 (2003) 4985.
- [32] N.A. Bhole, I.D. Johnson, K.M. Keville, Q.N. Le, G.H. Yokomizo, *US Patent 5,260,501* (1993) Mobil Oil Corporation.
- [33] E. Rodríguez-Castellón, L. Díaz, P. Maireles-Torres, A. Jiménez-López, A. Vaccari, *Appl. Catal. A: Gen.* 240 (2003) 83.
- [34] A. Klemt, A. Taouli, H. Koch, W. Reschetilowski, *Stud. Surf. Sci. Catal.* 127 (1999) 405.
- [35] A. Klemt, W. Reschetilowski, *Chem. Eng. Technol.* 25 (2002) 137.
- [36] D. Eliche-Quesada, J. Mérida-Robles, P. Maireles-Torres, E. Rodríguez-Castellón, A. Jiménez-López, *Appl. Catal. A* 262 (2004) 111.
- [37] H-P. Lin, C-Y. Mou, *Science* 273 (1996) 765.
- [38] K. Chaudhari, T.K. Das, A.J. Chandwadkar, S. Sivasanker, *J. Catal.* 186 (1999) 81.
- [39] S. Biz, *J. Phys. Chem. B* 103 (1999) 8432.
- [40] S.C. Shen, S. Kawi, *J. Phys. B* 103 (1999) 8870.
- [41] N. Yao, C. Pinckney, S. Lim, C. Pak, G. Haller, *Micropor. Mesopor. Mater.* 44/45 (2001) 377.
- [42] R.H. Huesca, J.M. Robles, P.M. Torres, E.R. Castellón, A.J. López, *J. Catal.* 203 (2001) 122.
- [43] C. Minchev, S.A. Zubkov, V. Valtchev, V. Minkov, *Appl. Catal. A* 119 (1994) 195.
- [44] M.D. Romero, J.A. Calles, A. Rodriguez, *Ind. Eng. Chem. Res.* 36 (1997) 3533.

- [45] Yamagishik, I. Nakamura, S. Nakai, A. Iino, Proceedings of the 9th IZC, Montreal, Canada, 1992, RP68.
- [46] K. Fang, W. Wei, J. Ren, Y. Sun, *Catal. Lett.* 93 (2004) 235.
- [47] C.A. Emeis, *J. Catal.* 141 (1993) 347.
- [48] J. Weitkamp, *Ind. Eng. Chem. Chem. Prod. Res. Dev.* 21 (1982) 550.
- [49] M.L. Conrads, W.E. Garwood, *Ind. Eng. Chem. Prod. Res. Dev.* 20 (1981) 654.
- [50] P.B. Weisz, *Adv. Catal.* 13 (1962) 137.
- [51] C. Nie, L. Huang, D. Zhao, Q. Li, *Catal. Lett.* 71 (2001) 117.
- [52] W. Zhang, P.G. Smirniotis, *J. Catal.* 182 (1999) 400.